Applied Acoustics 103 (2016) 54–63

Contents lists available at ScienceDirect

Applied Acoustics

journal homepage: www.elsevier.com/locate/apacoust

# Multi-channel time frequency shift keying in underwater acoustic communication

Xiaoyi Hu [a,b], Deqing Wang [a,b,*], Yurong Lin [a,b], Wei Su [a,b], Yongjun Xie [a,b], Longcheng Liu [c]

[a] Department of Communication Engineering, School of Information Science and Engineering, Xiamen University, Xiamen 361005, PR China
[b] Key Laboratory of Underwater Acoustic Communication and Marine Information Technology (Xiamen University), Ministry of Education, Xiamen 361005, PR China
[c] School of Mathematical Sciences, Xiamen University, Xiamen 361005, PR China

ARTICLE INFO

*Article history:*
Received 17 June 2015
Received in revised form 14 September 2015
Accepted 14 October 2015
Available online 28 October 2015

*Keywords:*
Time frequency shift keying
Underwater acoustic communication
Long-range

ABSTRACT

Current long-range underwater acoustic communication (UWAC) faces many difficulties such as great propagation loss, high ambient noise and long multi-path delay. In order to design an excellent long-range UWAC system, it is necessary to increase signal-to-noise ratio (SNR), suppress inter-symbol interference (ISI) and alleviate frequency selective fading. In this paper, a novel time frequency shift keying scheme named as Multi-channel Hex Four Time Four Frequency Shift Keying (McH-4T4FSK) is presented. Both theoretical analysis and simulation over Bellhop multi-path channel model indicate that McH-4T4FSK exhibits lower bit error rate (BER) at the same SNR compared with traditional Frequency Shift Keying (FSK) regardless of diversity or not. Moreover, shallow water sea trial experiments at Xiamen Port with 15 km distance and at Taiwan Strait with 30 km distance confirm that McH-4T4FSK possesses lower BER and better robustness.



## 1. Introduction

With the rapid development of oceanography, maritime research, offshore oil exploration and maritime defense system in the last three decades, modern cooperative communication network between underwater and land has become an urgent need for efficient information sharing and convenient information communication [1,2]. Generally, underwater acoustic channels are recognized as one of the most difficult communication media in practice today, and there are many obstacles in developing applicable products although recent research has improved the performance and reliability of the UWAC system [3]. Undoubtedly, how to realize remote and robust UWAC system is a pressing problem for overcoming these obstacles.

In order to get robust UWAC system, many developing applications, both commercial and military ones, are prone to choose non-coherent modulation as their preferred solutions. Non-coherent detection of multi- frequency shift keying (MFSK) signals has traditionally been considered as the only alternative for channels with rapid phase variation, such as the long and medium range channels of shallow water [4]. Ref. [5] introduced a kind of communication scheme called as fast frequency-hopped/M-ary frequency shift keying (FFH/MFSK) in order to realize deep-sea remote communication, in which the MFSK signals were modulated twice through the technique of fast frequency hopping so as to suppress frequency selective fading caused by multi-path propagation. Ref. [6] proposed a novel frequency group coding (FGC) method different from traditional MFSK frames, in which the neighboring MFSK symbols were mapped to different frequency groups so as to effectively restrain the severe multi-path. Ref. [7] presented an optimal high speed adaptive multi-carrier UWAC system based on MFSK modulation, and relevant experiments in a lake confirmed its suitability for high speed multi-carrier UWAC system between 10 and 30 km medium range in severe acoustic channels. Considering the good performance of time frequency shift keying (TFSK) against multi-path interference, Ref. [8] explored the effect of TFSK modulation in UWAC system, and the results demonstrated its feasibility for UWAC over a distance of 5 km at a data transmission rate of 1 k bits/s.

This paper presents a novel TFSK modulation named as Multi-channel Hex Four Time Four Frequency Shift Keying (McH-4T4FSK) which includes four time slots and four frequencies. The meaning of multi-channel is that there are multiple independent physical narrow band channel with the same bandwidth and different center frequencies at receiver. The received signal at each time slot passes the multiple channels all the same time. The

* Corresponding author at: Department of Communication Engineering, School of Information Science and Engineering, Xiamen University, Xiamen 361005, PR China.
*E-mail address:* deqing@xmu.edu.cn (D. Wang).

http://dx.doi.org/10.1016/j.apacoust.2015.10.009
0003-682X/

scheme is characterized by two aspects: high-array modulation at the transmitter to improve spectral efficiency and multi-channel processing at the receiver to enhance the SNR of received signals. Hence, the UWAC system not only inherits anti-fading ability from TFSK communication system, but also can effectively extract signals from strong ambient noise due to its multiple narrow band channels.

The rest of this paper is organized as follows. In Section 2, the underwater acoustic signal propagation model is introduced. Then, Section 3 describes the novel TFSK scheme from frequency mapping, modulation and processing at receiver. In Section 4, the performance of the TFSK scheme is analyzed at Rayleigh fading channel. In Section 5, the numerical analysis results of Section 4 are provided, and meanwhile the scheme is simulated over BELLHOP multi-path channel based on beam tracing model. Furthermore, Section 6 presents sea trial results and analyzes the signals and experiment results. Finally, Section 7 summarizes this paper.

## 2. Underwater acoustic signal propagation model

In general, underwater acoustic signals are influenced by the ambient noise and the multi-path propagation effect. The ambient noise affects SNR directly, while the impact of multi-path propagation can result in amplitude fading and ISI of acoustic signals.

The ambient noise in the ocean can be modeled using four sources: turbulence, shipping, waves, and thermal noise. Among these forces, surface motion caused by wind-driven waves is the major factor contributing to the noise in the frequency region of 100 Hz – 100 kHz, which is the operating region of most acoustic systems. It is noted that most of the ambient noise sources can be described by Gaussian statistics and a continuous power spectral density (p.s.d.) [9].

Multi-path formation in the ocean is governed by two aspects: one is sound reflection at the surface, bottom and any other objects, and the other is sound refraction in the water. Since sound refraction is a consequence of the spatial variability of sound speed [10], underwater acoustic propagation signals can actually be viewed as a kind of complex random process. Ref. [11] established a time-varying underwater acoustic channel based on the ray theory, and eigen-rays corresponding to direct or reflected multi-path can be determined using ray tracing. Considering these discrete multi-path, a time-varying channel impulse response (CIR) can be represented as:

$$h(\tau,t)=\sum_{i=1}^{N}a_i(t)\delta[t-\tau_i(t)] \tag{1}$$

where $N$ is the number of multi-path, $a_i(t)$ is the amplitude attenuation factor of $i$th path and $\tau_i(t)$ is the $i$th path delay.

Considering the combined effects of additive noise and multi-path propagation, the signal denoted by $y(t)$ at the receiving end can be obtained through Eq. (2):

$$y(t)=h(t)*x(t)+n(t) \tag{2}$$

where $x(t)$ is the transmit signal, and $n(t)$ is the Additive White Gaussian Noise (AWGN).

When the maximum delay is shorter than the period of symbol, the channel can be regarded as Rayleigh-type fading channel. Section 4 presents the performance analysis for this kind of channel. When the maximum delay is longer than the period of symbol, the channel is a kind of complicated multi-path channel, and it is difficult to draw a closed solution in this case. In view of this, Section 5 provides the simulation results based on Bellhop channel, which is a kind of typical multi-path channel model used in UWAC system simulation.

## 3. McH-4T4FSK scheme

Traditionally, various techniques are used to achieve diversity effects for the purpose of anti-fading. However, space diversity needs several antennas while frequency diversity may disperse the limited transmitter power. Fortunately, TFSK modulation can overcome those drawbacks without increasing the number of antenna or dispersing transmitter power. In this section, we will introduce the system design from three aspects of frequency mapping, modulation, and processing at the receiver.

### 3.1. Frequency mapping

Similar to 16-ary FSK modulation scheme, the available frequency band resource is divided into sixteen frequency points. Further, these frequency points are grouped into four different physical sub-channels and there are four frequency points in each physical sub-channel. The approach brings two advantages. One is to improve the SNR of the received signals because of sub-channel's narrower bandwidth. On the other hand, the frequency points in adjacent time slots come from different physical sub-channels, as a result, the interference between adjacent time slots within a symbol could be highly suppressed. Based on the above ideas, the frequency points are noted as $f_{IJ}(1\leqslant I\leqslant 4, 1\leqslant J\leqslant 4)$, where $J$ is to represent the physical sub-channel number, namely, *No. of Channel*, and $I$ is to represent the order of frequency points within each physical sub-channel, namely, *No. in Channel*. Table 1 shows the frequency mapping $f_{IJ}$.

Based on the frequency mapping shown in Table 1, transmission symbols can be encoded by frequency groups, which will be described in Section 3.2.

### 3.2. Modulation

TFSK modulation uses signals consisting of orthogonal frequencies to denote information bits during the transmission period [12]. For example, 2-ary TFSK modulation uses two frequency signals to denote bit '0' and the other two frequency signals to denote bit '1'. Thus, a binary period is divided into two time slots with the same width. When bit '0' is transmitted, the first time slot is filled with frequency $f_1$ and the second time slot is filled with frequency $f_2$; when bit '1' is transmitted, frequency $f_2$ is transmitted firstly and frequency $f_1$ is transmitted secondly.

Similarly, in McH-4T4FSK modulation, four binary bits form a symbol and each symbol period is divided into four time slots averagely. Each time slot is filled with a frequency signal selected from a special frequency group. The frequency group is composed by four different frequency signals. The encoding map between symbols and frequency groups can be seen in Table 2.

The encode mapping shown in Table 2 indicates that McH-4T4FSK is characterized by the following aspects. First, each symbol has different frequency point in different time interval, which enhances the ability of anti-fading. Second, the frequency points in each symbol come from different sub-channels, which improves the capability of anti-interference within a symbol. Last,

**Table 1**
Frequency mapping.

| No. of Channel | No. in Channel | | | |
|---|---|---|---|---|
| | $I=1$ | $I=2$ | $I=3$ | $I=4$ |
| $J=1$ | $f_{11}$ | $f_{21}$ | $f_{31}$ | $f_{41}$ |
| $J=2$ | $f_{12}$ | $f_{22}$ | $f_{32}$ | $f_{42}$ |
| $J=3$ | $f_{13}$ | $f_{23}$ | $f_{33}$ | $f_{43}$ |
| $J=4$ | $f_{14}$ | $f_{24}$ | $f_{34}$ | $f_{44}$ |

**Table 2**
Encoded by frequency group table.

| Symbol | Frequency group | Symbol | Frequency group |
|---|---|---|---|
| 0000 | $f_{11}f_{12}f_{13}f_{14}$ | 1000 | $f_{31}f_{32}f_{33}f_{34}$ |
| 0001 | $f_{12}f_{14}f_{11}f_{13}$ | 1001 | $f_{32}f_{34}f_{31}f_{33}$ |
| 0010 | $f_{13}f_{11}f_{14}f_{12}$ | 1010 | $f_{33}f_{31}f_{34}f_{32}$ |
| 0011 | $f_{14}f_{13}f_{12}f_{11}$ | 1011 | $f_{34}f_{33}f_{32}f_{31}$ |
| 0100 | $f_{21}f_{22}f_{23}f_{24}$ | 1100 | $f_{41}f_{42}f_{43}f_{44}$ |
| 0101 | $f_{22}f_{24}f_{21}f_{23}$ | 1101 | $f_{42}f_{44}f_{41}f_{43}$ |
| 0110 | $f_{23}f_{21}f_{24}f_{22}$ | 1110 | $f_{43}f_{41}f_{44}f_{42}$ |
| 0111 | $f_{24}f_{23}f_{22}f_{21}$ | 1111 | $f_{44}f_{43}f_{42}f_{41}$ |

the frequency points in the same time interval of each symbol are orthogonal with that of other symbol, which improves the capability of anti-interference between the different symbols.

### 3.3. Processing at receiver

At the receiving end, there are four physical sub-channels with different bandwidth, a Time Delay Matrix, sixteen combiners and a decider. The receiving structure is shown in Fig. 1.

Received signal at one time slot firstly passes through four sub-channels, which are denoted as Sub-channel 1#, Sub-channel 2#, Sub-channel 3# and Sub-channel 4# in Fig. 1. Each physical sub-channel is composed of a band-pass filter with different bandwidth, a synchronization unit and four correlators. The physical sub-channel is shown in Fig. 2.

The most front end of the physical sub-channel is a band-pass filter with different bandwidth. For example, the frequency bands at these sub-channels are 2–3 kHz, 3–4 kHz, 4–5 kHz and 5–6 kHz respectively in McH-4T4FSK system. Compared with the whole bandwidth (4 kHz) of the communication system, the bandwidth of the sub-channel (1 kHz) is much narrower. It is good for improving SNR of the received signals especially in long-range UWAC environment. Furthermore, the bandwidth of band-pass filter at each sub-channel is different. It is good for suppressing interference from other sub-channel's signals. After passing the individual band-pass filter, the narrow-band received signal is synchronized respectively followed by a frequency signal demodulator. Because there are four frequency points at each sub-channel, the demodulator is composed of four correlators corresponding to four frequency points. These correlators are denoted as Correlator 1#, Correlator 2#, Correlator 3# and Correlator 4# in Fig. 2. Then, the outputs of the correlators are four peak values. At AWGN environment, the output of the correlator with the same frequency as received signal is higher than the others.

Since a symbol is composed of four time slots or four consecutive frequency points, the symbol cannot be decoded until four time slots are provided later. Then a Time Delay Matrix shown in Fig. 1 is created to cache the outputs of the correlators. For a sub-channel, there are four output peak values corresponding to four frequency points at each time slot. From this respect, every time cache should save four peak values.

Four consecutive time slots later, each combiner get four peak values from Time Delay Matrix according to symbol encoding rule. There are sixteen combiners denoted as Combiner 1# to Combiner 16# in Fig. 1. These combiners and encoded symbols are one-one correspondence. For example, if the encoded symbol is "0000", according to Table 2, the four ordered signals are $f_{11}$, $f_{12}$, $f_{13}$ and $f_{14}$. It means that Combiner 1# gets the peak value at the first time slot from Sub-channel 1#, at the second time slot from Sub-channel 2#, at the third time slot from Sub-channel 3# and at the fourth time slot from Sub-channel 4#. The process of getting peak values is denoted by the arrows pointing to Combiner 1# in Fig. 1. Different from the symbol "0000", if the encoded symbol is "0101" which corresponds to Combiner 6#, according to Table 2, the four ordered signals are $f_{22}$, $f_{24}$, $f_{21}$ and $f_{23}$. It means that Combiner 6# gets the peak values sequentially from Sub-channels 2#, 4#, 1# and 3# at the four time slots.

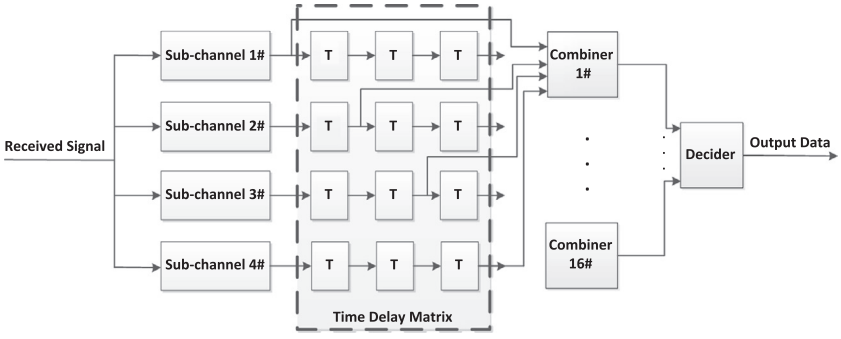


**Fig. 1.** The receiving structure.

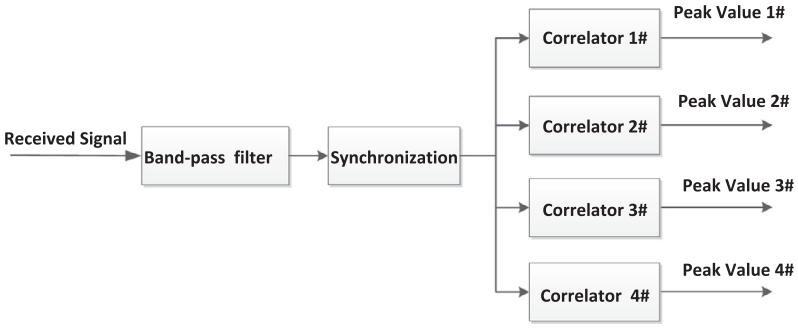


**Fig. 2.** The physical sub-channel.

After each combiner gets four peak values and sums them up, the decider which is denoted as Decider in Fig. 1 selects the maximum value as the decoded symbol. According to Table 2, the source data can be decoded.

## 4. Performance analysis

In this section, the performance of McH-4T4FSK system in an interference environment will be considered [13]. According to Fig. 1, there are four peak values entering into each combiner. For a special transmitting symbol, the inputs of different combiners are different and only a special combiner receives the information of transmitting symbol. Here, the inputs carrying transmitting information are defined as $V_1^2$ $V_2^2$, $V_3^2$ and $V_4^2$, while those only carrying noise are defined as $v_1^2$, $v_2^2$, $v_3^2$ and $v_4^2$. Then, the input to the Decider will be in the form of

$$y_D = \sum_{i=1}^{4}(V_i^2 - v_i^2) \tag{3}$$

It is common to say that the short-range underwater channel is modeled as Rice distribution and the long-range one is modeled as Rayleigh distribution [14–16]. So the following performance analysis is discussed by two aspects, one is with white noise but no fading and the other is with both noise and fading.

(a) With white noise but no fading

The probability distribution function (PDF) for $V_i$ is given by the result of Rice:

$$p(V_i) = \begin{cases} \left(\frac{V_i}{\sigma^2}\right) e^{-\frac{V_i^2+A_i^2}{2\sigma^2}} I_0\left(\frac{A_i V_i}{\sigma^2}\right) & V_i \geqslant 0 \\ 0 & V_i < 0 \end{cases} \tag{4}$$

where $\sigma^2$ is the average noise power, and $A_i$ is the signal amplitude. The PDF for an envelope sample of noise $v_i$ is given by the Rayleigh distribution:

$$p(v_i) = \begin{cases} \left(\frac{v_i}{\sigma^2}\right) e^{-\frac{v_i^2}{2\sigma^2}} & v_i \geqslant 0 \\ 0 & v_i < 0 \end{cases} \tag{5}$$

For the convenience of description, the following notations are introduced:

$$\begin{cases} X_i = (V_i/\sqrt{2}\sigma)^2 \\ x_i = (v_i/\sqrt{2}\sigma)^2 \\ K_i = (A_i/\sqrt{2}\sigma)^2 \end{cases} \tag{6}$$

Then, it can be obtained that

$$y = (y_D/\sqrt{2}\sigma)^2 = \sum_{i=1}^{4}(X_i^2 - x_i^2) \tag{7}$$

Thus, Eqs. (4) and (5) can be rewritten as:

$$p(X_i) = \begin{cases} e^{-(X_i+K_i)} I_0(2\sqrt{X_i \cdot K_i}) & X_i \geqslant 0 \\ 0 & X_i < 0 \end{cases} \tag{8}$$

$$p(x_i) = \begin{cases} e^{-x_i} & x_i \geqslant 0 \\ 0 & x_i < 0 \end{cases} \tag{9}$$

Under the assumption of no fading in the channel, the signals of amplitude $A_i (1 \leqslant i \leqslant 4)$ are supposed to be the same value $A$; meanwhile, $K_1 = K_2 = K_3 = K_4 = K$.

The average digit-error probability is given by

$$P_e^0 = P\{y < 0\} = P\left\{\left(\sum_{i=1}^{4} X_i - \sum_{i=1}^{4} x_i\right) < 0\right\} \tag{10}$$

In general, it is very difficult to get the PDF of $y$. However, since only the PDF for negative values of $y$ are concerned, the required PDF can be found deduced from an important relation developed by Marcum [17]:

$$p(y) = \frac{e^{y-2r}}{32}\left[-\frac{y^3}{3} + \frac{y^2}{2}(2r+4) - y(r^2+5r+5) + \frac{1}{3}r^3 + 3r^2 + \frac{15}{2}r + 5\right] \tag{11}$$

where $r = \frac{A^2}{2\sigma^2}$ is SNR. Thus, the average digit-error probability can be expressed as:

$$P_e^0 = \int_{-\infty}^{0} p(y)dy = \frac{e^{-2r}}{32}\left[\frac{1}{3}r^3 + 4r^2 + \frac{29}{2}r + 16\right] \tag{12}$$

Based on the symbol error rate, the BER of 16-ary modulation can be obtained as [18]:

$$P_b^0 = \frac{8}{15}P_e^0 = \frac{e^{-2r}}{60}\left[\frac{1}{3}r^3 + 4r^2 + \frac{29}{2}r + 16\right] \tag{13}$$

(b) With both white noise and fading

Here, the signals into the detectors are assumed to be subjected to slow Rayleigh-type fading.

The PDF for the signal amplitude $A_i$ is given by:

$$p(A_i) = \begin{cases} \left(\frac{2A_i}{A_0^2}\right) e^{-\frac{A_i^2}{A_0^2}} & A_i \geqslant 0 \\ 0 & A_i < 0 \end{cases} \tag{14}$$

where $A_0^2$ is the mean square amplitude of the signals.

Assuming that the frequency separation between channels is sufficient to assure independent fading, then the average digit-error probability is:

$$P_e^1 = \int\int\int\int_0^{\infty} p(A_1, A_2, A_3, A_4) P_e^0 dA_1 dA_2 dA_3 dA_4 \tag{15}$$

where $p(A_1, A_2, A_3, A_4)$ is the joint PDF of the signal amplitude. Considering the independence of fading, it can be obtained that

$$p(A_1, A_2, A_3, A_4) = \prod_{i=1}^{4} p(A_i) \tag{16}$$

Using Eqs. (14–16), it can be obtained that

$$P_e^1 = \frac{1}{2(2+r)^4}\left[\left(\frac{r}{2+r}\right)^3 + \frac{33}{4(2+r)^2}r^2 + \frac{29}{2+r}r + \frac{1}{8} + 19\right] \tag{17}$$

where $r = \frac{A_0^2}{2\sigma_n^2}$ is the average SNR of signals into the detector.

Similar to Eq. (13), the BER in fading channel can be expressed as:

$$P_b^1 = \frac{8}{15}P_e^1 = \frac{4}{15(2+r)^4}\left[\left(\frac{r}{2+r}\right)^3 + \frac{33}{4(2+r)^2}r^2 + \frac{29}{2+r}r + \frac{1}{8} + 19\right] \tag{18}$$

As a comparison, we get the BER of 16-ary FSK without diversity (named as 16FSK) and with two-branch diversity (named as D2-16FSK) over Rayleigh channel [19,20]. The BER of 16FSK with non-coherent detection is as follows:

$$P_b^{16FSK} = \frac{1}{2}\frac{M}{M-1}\sum_{m=1}^{M-1}(-1)^{n+1}\binom{M-1}{m}\frac{1}{m+1}\exp\left[-\frac{1}{m+1}\frac{kE_b}{N_0}\right] \tag{19}$$

where $P_b^{16FSK}$ is BER over Rayleigh channel, $\frac{E_b}{N_0}$ is the energy per bit ($E_b$)-to-noise power spectral density ($N_0$) ratio, $M$ is the size of modulation constellation and $k$ is the number of bits per symbol. As for 16FSK, $M$ is 16 and $k$ is 4.

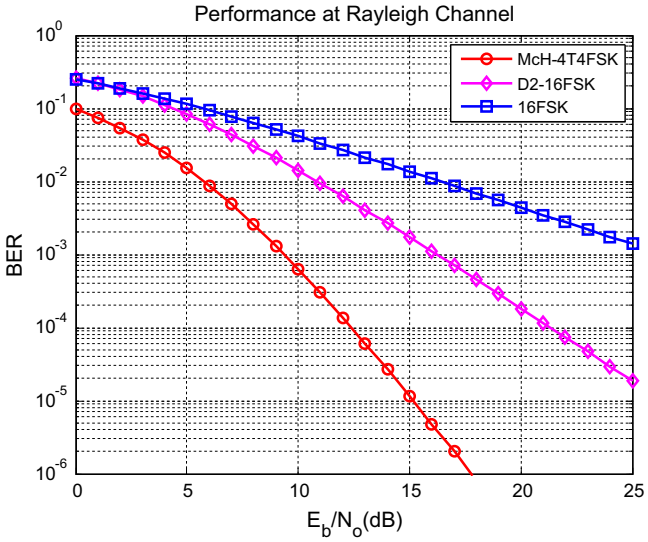


**Fig. 3.** Dependence of BER on $\frac{E_b}{N_0}$ for different schemes over Rayleigh channel.

**Table 3**
Parameters of Bellhop channel table.

| Simulation parameters | Value |
|---|---|
| Source depth/m | 20 |
| Receiver depth/m | 10 |
| Depth/m | 50 |
| Distance/km | 10 |
| Central frequency/kHz | 3.5 |
| RMS roughness of top interface of layer (m) | 2 |
| Vector of compressional sound speed (m/s) | 1517–1518 |

The BER of D2-16FSK with non-coherent detection is as follows:

$$P_b^{\text{D2-16FSK}} = \frac{1}{2}\frac{M}{M-1}\left\{1 - \int_0^{\infty} \frac{1}{(1+\bar{\gamma})^L (L-1)!} U^{L-1} \times e^{-\frac{U}{1+\bar{\gamma}}}\left(1 - e^{-U}\sum_{k=0}^{L-1}\frac{U^k}{k!}\right)^{M-1} dU\right\} \quad (20)$$

where $P_b^{\text{D2-16FSK}}$ is BER over Rayleigh channel, $\frac{E_b}{N_0}$ is the energy per bit ($E_b$)-to-noise power spectral density ($N_0$) ratio, $\bar{\gamma}$ is the SNR per symbol per branch, $L$ is the number of diversity branches. $M$ is the size of modulation constellation and $k$ is the number of bits per symbol. As for D2-16FSK, $L$ is 2, $M$ is 16 and $k$ is 4.

## 5. Numerical analysis and simulation

Based on analysis in Section 4, Fig. 3 illustrates the performance difference of McH-4T4FSK, 16FSK and D2-16FSK over Rayleigh channel. The curves are drawn by referring to Eq. (18), Eqs. (19) and (20) respectively. Notably, the parameter $r$ in Eq. (18) is actually the mean of $\frac{E_b}{N_0}$.

At the same $\frac{E_b}{N_0}$, BER of McH-4T4FSK is significantly lower than those of 16FSK and D2-16FSK. Meanwhile, because of the nonlinear increase of SNR gain, the performance of D2-16FSK is better than that of 16FSK. When $\frac{E_b}{N_0}$ is 0 dB, BER of McH-4T4FSK is at the level of $10^{-2}$. As discussed in the Section 2, UWAC channel is regarded as Rayleigh channel when the maximum delay is shorter than the period of symbol. Therefore, it can be concluded that McH-4T4FSK scheme is suitable for UWAC system when the maximum delay is shorter than the period of symbol.

On the other hand, when the maximum delay is longer than the period of symbol, the UWAC channel is equivalent to the FIR filter described in Eq. (1). In this case, Bellhop is a beam tracing model widely used in computer simulation. According to the environment of Taiwan Strait (with an average depth of 50 m), the parameter settings shown in Table 3 are adopted.

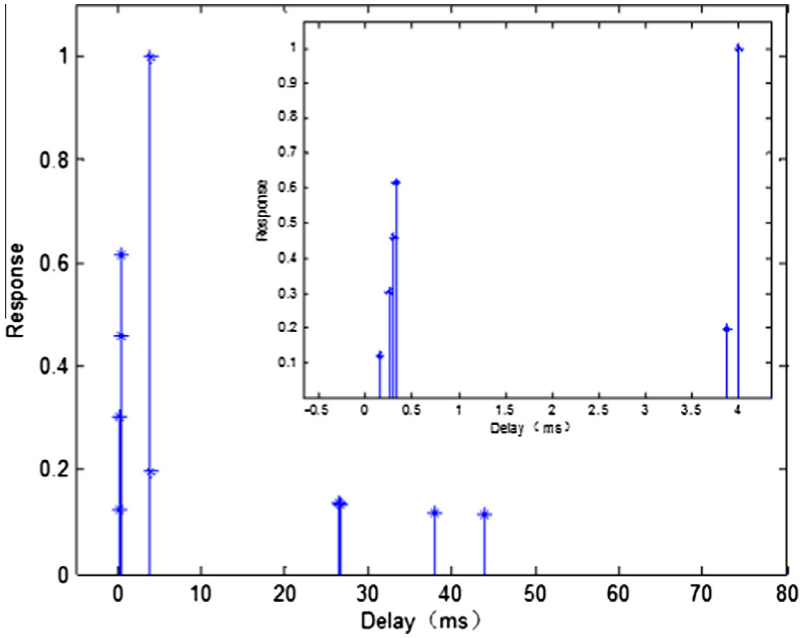


**Fig. 4.** CIR over Bellhop channel model.

Fig. 4 shows the Bellhop CIR based on the above parameter settings. As can be seen, the strongest path is not the direct way and the maximum delay is more than 40 ms.

Let McH-4T4FSK, D2-16FSK and 16FSK systems pass through the shallow water channel respectively. The four band channels are set as 2–3 kHz, 3–4 kHz, 4–5 kHz and 5–6 kHz. For McH-4T4FSK and 16FSK systems, there are four frequencies in each channel. For example, in 2–3 kHz channel, the four frequencies are 2.2 kHz, 2.4 kHz, 2.6 kHz and 2.8 kHz. Similar frequency allocation is conducted in other three channels. For D2-16FSK system, there are eight frequencies in each channel, and the frequency allocation rule is similar to that for McH-4T4FSK and 16FSK systems. In numerical simulation, the traffic data are $10^7$ bits and the communication rate is 100 bit/s. Fig. 5 illustrates the BER performance of different systems. As can be seen, Mch-4T4FSK is characterized by lower BER compared with D2-16FSK and 16FSK systems, but higher SNR is needed at multi-path environment compared with AWGN environment.

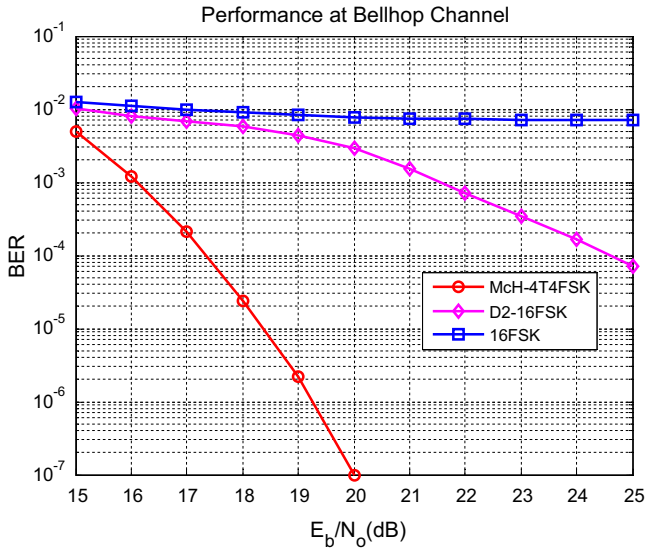


**Fig. 5.** Dependence of BER on $\frac{E_b}{N_0}$ for different schemes over Bellhop channel.

To sum up, Mch-4T4FSK scheme is more reliable than traditional schemes such as D2-16FSK and 16FSK no matter over Rayleigh channel or multi-path channel.

## 6. Experiments

A number of field trials were carried out at Xiamen Port in January and June, 2014 and at Taiwan Strait in June, 2014. The objective of these experiments was to test the performance of McH-4T4FSK scheme.

### 6.1. Setup of sea trial

Fig. 6 shows the deployment of sea trial at Xiamen Port in January and June, 2014. The distance between the sender and the receiver is 15 km and the depth is 17 m. A commercial cylindrical transducer deployed at the depth of 8 m was used as the acoustic transmitter, while a spherical transducer deployed at the same depth as the source was used as the acoustic receiver. The source can provide a source level of more than 190 dB when it works at 2–6 kHz, while its receiving sensitivity is −187 dB which is higher than normal hydrophone. The sea conditions of the two sea trials at Xiamen Port are both so severe that the scale level is measured as 5.

Fig. 7 shows the deployment of sea trial at Taiwan Strait in July, 2014. The distance between the sender and the receiver is 30 km and the depth is 50 m. The transmitter and receiver are identical to those used at Xiamen Port, but they were deployed at the depth of 30 m since the ocean depth is much deeper. The wind speed is from 5 to 11 m/s, which is equivalent to the scale level of 3 to 5.

The frequency band of transmitted signals varied from 2 to 6 kHz with 100 bits per sencond (bps). With a fixed transmission source level, the source consecutively broadcasted the signals as shown in Fig. 8. The received signals were collected by NI DAQ (NI USB-6259) for off-line processing in the laboratory. Four


**Fig. 6.** Deployment of sea trial at Xiamen Port in January and June, 2014.

identical LFM signals with a bandwidth of 1 kHz and a time duration of 2 s were used as sub-channel time synchronization. The length of synchronization signal was so long that the signal could be separated accurately. At the same time, the synchronization signal was used for CIR estimation. The data signals are equipped with McH-4T4FSK scheme, and each symbol consists of four frequencies from four different sub-channels. Each frequency signal lasts 0.01 s and the sub-channels at the receiver could get the corresponding signals through their synchronization signals. Otherwise, the tones ahead of the frame were used to test channel conditions.

In order to facilitate access, we list the parameters of McH-4T4FSK communication system at sea trials in Table 4.

**Table 4**
The parameters of McH-4T4FSK at sea trials.

| Parameters/unit | Value |
|---|---|
| Bandwidth of the whole system/kHz | 2–6 |
| Bandwidth of sub-channel 1#/kHz | 2–3 |
| Bandwidth of sub-channel 2#/kHz | 3–4 |
| Bandwidth of sub-channel 3#/kHz | 4–5 |
| Bandwidth of sub-channel 4#/kHz | 5–6 |
| Sample rate/kHz | 40 |
| Period of each time slot/ms | 10 |
| Transmission distance/km | 15(Xiamen Port), 30(Taiwan Strait) |
| Scale level of sea state | 5(Xiamen Port), 3–5(Taiwan Strait) |
| Bit rate/bps | 100 |
| Transmitted source data/bits | 4096 |

### 6.2. Analysis of signal and experiment results

Fig. 9 shows CIR estimations at Xiamen Port and Taiwan Strait. The CIR is represented by $h(t,\tau)$ in the figure, where $t$ represents the test time and $\tau$ represents the delay time. At the same time, the magnitude of the impulse response is normalized. We can find that the results of CIRs vary greatly at different locations and at different testing time from Fig. 8. The channel at Xiamen Port is characterized by significant direct path, weak multi-path and low ambient noise during the sea trial period. The maximum delay time of multi-path is shorter than 20 ms. By contrast, at Taiwan Strait there are no obvious direct ways and several paths of near equivalent gains arrive within 10 ms. The maximum delay time between two paths is more than 50 ms. Furthermore, the ambient

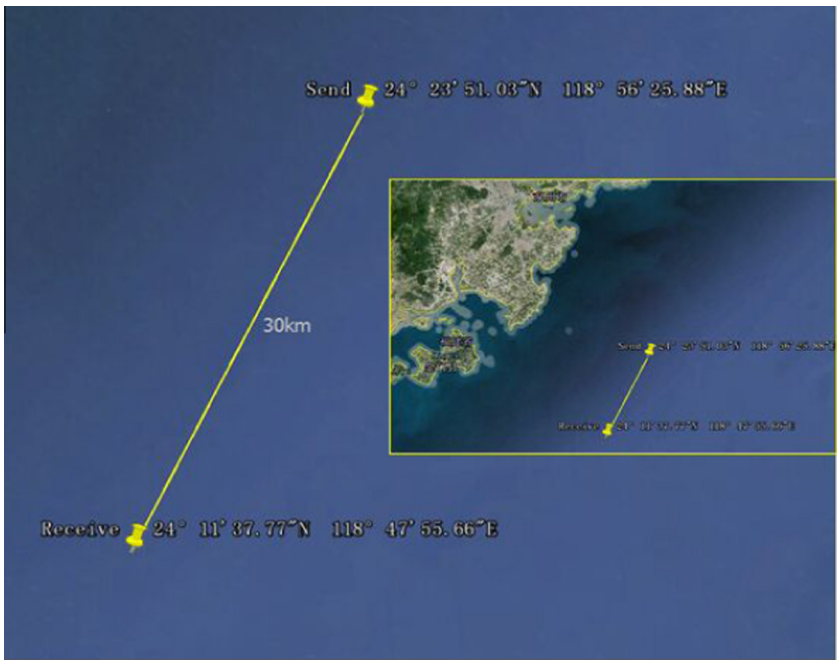


**Fig. 7.** Deployment of sea trial at Taiwan Strait in July, 2014.

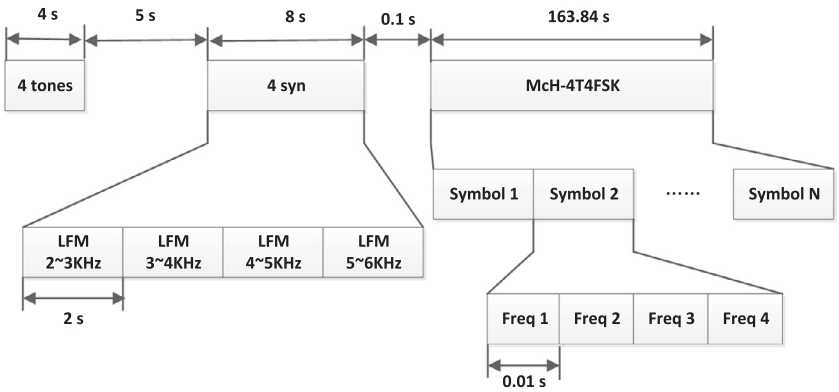


**Fig. 8.** Diagram for transmitted signals.

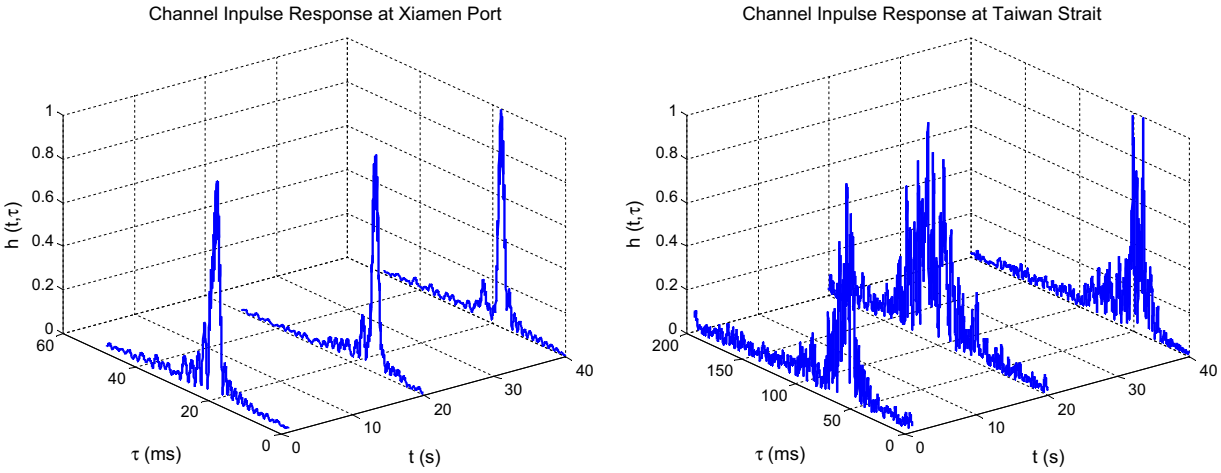


(a) At Xiamen Port (b) At Taiwan Strait

**Fig. 9.** CIR estimations at Xiamen Port and Taiwan Strait.

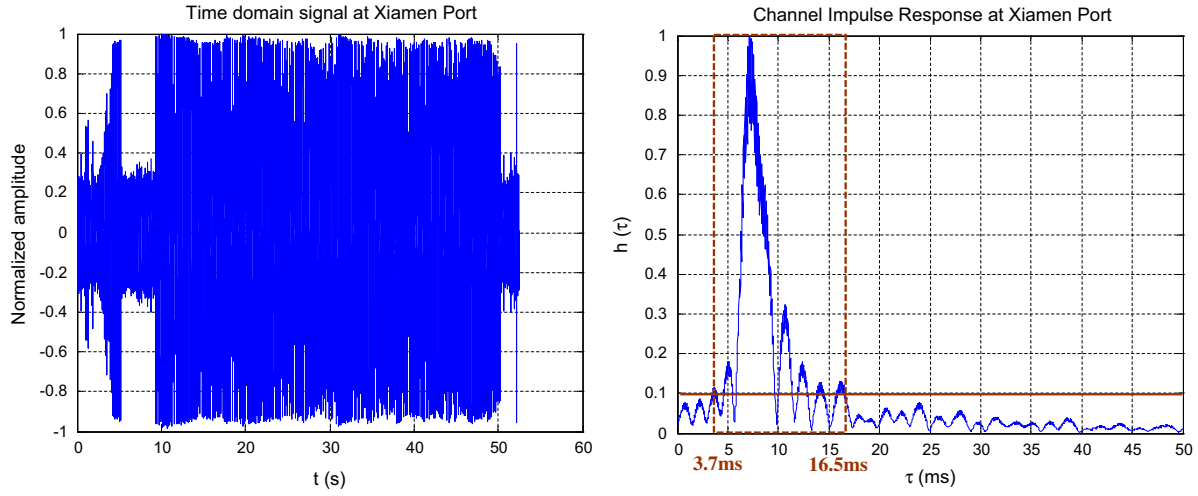


(a) Signal with high SNR (b) CIR with short multi-path

**Fig. 10.** Time-domain signal and CIR at Xiamen Port.

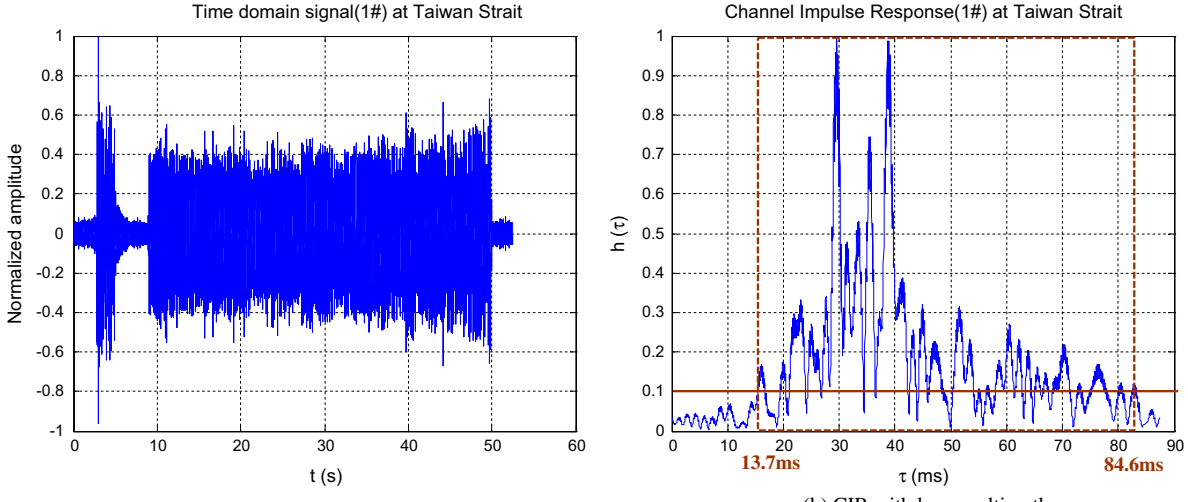


(a) Signal with high SNR (b) CIR with long multi-path

**Fig. 11.** Time-domain signal and CIR (1#) at Taiwan Strait.

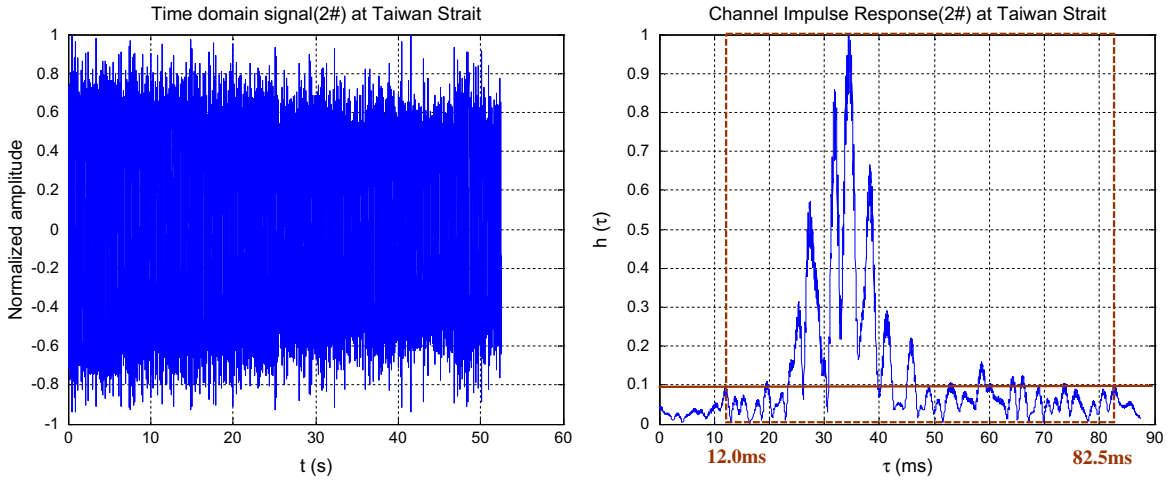


(a) Signal with low SNR

(b) CIR with long multi-path

**Fig. 12.** Time-domain signal and CIR (2#) at Taiwan Strait.

noise at Taiwan Strait is much higher than the one at Xiamen Port. These CIRs are representative for different channel configurations in communication. The channels at Xiamen Port are close to the Rice channel model with a direct path discussed in Section 4, while the channels at Taiwan Straight are close to Rayleigh-type fading model without a direct path. So it seems that the real field experiments have met with various of channel modes and the robustness of McH-4T4FSK scheme can be tested effectively although the number of field experiments is not numerous.

If individual received signal and its corresponding CIRs are concerned, it can be found that there are three kinds of typical signals in these sea trials. Fig. 10 shows a set of time-domain signal and the corresponding CIR at Xiamen Port sea trial. The time-domain signal is characterized by high SNR and short multi-path delay. The maximum delay time between the two paths is shown in Fig. 10(b) by dotted rectangle. When the normalized magnitude of multi-path drops to 0.1, the earliest arriving path is at the position of 3.7 ms and the latest one is at the position of 16.5 ms. Thus, the maximum delay time between the two path is 12.8 ms which is equivalent to a time slot. As a result, the received signals are with less multi-path interference. The BER ($2.4 \times 10^{-3}$) also verifies the point.

Figs. 11 and 12 show the time-domain signals and their corresponding CIRs at Taiwan Strait. The maximum delay time between the two paths are shown in Figs. 11(b) and 12(b) by dotted rectangle. There are long multi-path at Taiwan Straight at different time observed from 1# signal and 2# signal. For 1# signal, the earliest arriving path is at the position of 13.7 ms and the latest one is at the position of 84.6 ms. Thus, the maximum delay time between the two path is 70.9 ms. For 2# signal, the earliest arriving path is at the position of 12.0 ms and the latest one is at the position of 82.5 ms. Thus, the maximum delay time between the two path is 70.5 ms. Obviously, the maximum delay time is much longer than a time slot and even a symbol of McH-4T4FSK at Taiwan Strait . But in the case of the same multi-path delay, the BER performance of McH-4T4FSK is different for SNRs. The signals of higher SNR are with lower BER. For example, the BER of 1# signal with higher SNR is $2.9 \times 10^{-3}$ while the BER of 2# signal with lower SNR is $4.4 \times 10^{-2}$. We can draw a conclusion that McH-4T4FSK scheme has strong ability of resisting multi-path interference when the SNR is relatively high.

Table 5 presents the BER of McH-4T4FSK at sea trials. The number of transmitted data is 4096 bits so that the minimum BER is $2.4 \times 10^{-4}$. Limited by experimental conditions, the number of experiments is not numerous. But we can still find that McH-4T4FSK scheme is characterized by low BER whether at Xiamen Port or at Taiwan Strait. The BER on July 16th at Taiwan Strait is much higher than the others because the time-domain signal is with very low SNR denoted as Fig. 11.

Table 6 presents the average values of BER for the several experiments. Obviously, McH-4T4FSK scheme exhibits lower BER whether the sea trial is at Xiamen Port or at Taiwan Strait. Besides, it can be seen that the BER of McH-4T4FSK scheme keeps in the $10^{-3}$ level at any time. Therefore, it can be concluded that McH-4T4FSK scheme is a kind of robust communication scheme in the circumstances of high ambient noise and long multi-path delay.

**Table 5**
The BER of McH-4T4FSK at sea trials.

| Trial spot | Time | Order | BER |
|---|---|---|---|
| Xiamen Port | January 16th | 1 | $< 2.4 \times 10^{-4}$ |
| | June 7th | 1 | $5.6 \times 10^{-3}$ |
| | | 2 | $3.2 \times 10^{-3}$ |
| Taiwan Strait | July 13th | 1 | $< 2.4 \times 10^{-4}$ |
| | | 2 | $< 2.4 \times 10^{-4}$ |
| | | 3 | $< 2.4 \times 10^{-4}$ |
| | July 15th | 1 | $2.9 \times 10^{-3}$ |
| | | 2 | $8.1 \times 10^{-3}$ |
| | | 3 | $5.4 \times 10^{-3}$ |
| | July 16th | 1 | $4.4 \times 10^{-2}$ |

**Table 6**
The average BER comparison of several schemes.

| Trial spot | Time | McH-4T4FSK | D2-16FSK | 16FSK |
|---|---|---|---|---|
| Xiamen Port | January 16th | $< 2.4 \times 10^{-4}$ | $7.3 \times 10^{-3}$ | $3.6 \times 10^{-2}$ |
| | June 7th | $4.4 \times 10^{-3}$ | $3.4 \times 10^{-2}$ | $1.0 \times 10^{-1}$ |
| Taiwan Strait | July 13th | $< 2.4 \times 10^{-4}$ | $5.4 \times 10^{-3}$ | $1.2 \times 10^{-2}$ |
| | July 15th | $5.5 \times 10^{-3}$ | $1.1 \times 10^{-2}$ | $8.7 \times 10^{-2}$ |
| | July 16th | $4.4 \times 10^{-2}$ | $6.2 \times 10^{-2}$ | $1.2 \times 10^{-1}$ |

## 7. Conclusions

In summary, this paper presents a novel time frequency shift keying scheme McH-4T4FSK based on four time four frequency shift keying. The proposed scheme is characterized by three merits as follows. Firstly, the scheme can greatly suppress frequency selective fading owing to the two dimension diversity of its time-frequency. Secondly, there are four sub-channels with frequency band narrower than system band at the receiving end, so that the SNR is higher than single channel. Thirdly, the frequency at different time slot comes from different sub-channels, which enlarges the guard space and degrades the ISI. Both theoretical analysis and simulation over Bellhop multi-path channel model indicate that McH-4T4FSK scheme has lower BER (BER) at the same SNR compared with traditional Frequency Shift Keying (FSK) regardless of diversity or not. Moreover, shallow water sea trial experiments at Xiamen Port and Taiwan Strait confirm that McH-4T4FSK scheme has lower BER and better robustness. Therefore, McH-4T4FSK can provide a good reference for long-range UWAC system.

## Acknowledgements

The authors would like to thank the support from the teachers and students from UWAC lab in the sea trials. This work was supported by the National Natural Science Foundation of China (Grant Nos. 61301098, 61301097, 61471309, and 11001232) and Fujian Provincial Natural Science Foundation of China (Grant Nos. 2012J01021, 2013J01253, and 2013J01258).

## References

[1] Yoshida H, Hyakudome T, Ishibashi S, Ochi H, Asakawa K, Kasaya T, et al. Study on land-to-underwater communication. In: Wireless Personal Multimedia Communications (WPMC), 2011 14th International symposium on; 2011. Brest. p. 1–5.
[2] Xu Ke-ping, Xu Tian-zeng, Xu Ru, Cheng En, Wang Qing-chi, Nian Bao-qing. Underwater acoustic wireless communications. J Xiamen Univ (Natur Sci) 2001;40(2):311–9.
[3] Santoso Tri Budi, Wirawan Gamantyo Hendrantoro. Development of underwater acoustic communication model: opportunities and challenges. In: Information and Communication Technology (ICoICT), 2013 international conference of. Bandung; 2013. p. 358–62.
[4] Cai Hui-Zhi, Liu Yun-Tao, Cai Hui, Deng Hong-Chao, Wang Yong-Feng. Acoustic communication and its recent progress. Chin J Phys 2006;35(12):1038–43.
[5] Jiang Yu, Bai Xing-yu. Research on FFH/MFSK long range deep-water acoustic communication technique. Techn Acoust 2010;29(03):268–71.
[6] Wei Zhou-Fang, Huang Jian-Guo, He Cheng-Bing. Frequency group coding method to restrain the multipaths in MFSK long-range acoustic communications. Chin J Appl Acoust 2006;25(06):346–51.
[7] Wei Zhou-fang, Huang Jian-guo. MFSK based multi-carrier UWA communication system and lake experiment. Wireless Commun Technol 2006;02:9–13.
[8] Wang Yu, Hui Wang, Jinglin Xiang. On Exploring TFSK (Time Frequency Shift Keying) for improving underwater acoustic communication. J North West Polytech Univ 2004;22(5):635–9.
[9] Lucani DE, Stojanovic M, Medard M. On the relationship between transmission power and capacity of an underwater acoustic communication channel. In: OCEANS 2008 – MTS/IEEE Kobe Techno-Ocean. Kobe; 2008. p. 1–6.
[10] Stojanovic M, Preisig J. Underwater acoustic communication channels: propagation models and statistical characterization. Commun Magazine, IEEE 2009;47(1):84–9.
[11] Byun Sung-Hoon, Kim Sea-Moon, Lim Yong-Kon, Seong Woojae. Time-varying underwater acoustic channel modeling for moving platform. In: OCEANS 2007. Vancouver, BC; 2007. p. 1–4.
[12] Ma Dawei. A reliable data transmission scheme under wireless condition. In: Microwave and Millimeter Wave Technology, 2002. Proceedings. ICMMT 2002. 2002 3rd International conference on; 2002. p. 245–8.
[13] Splitt F. Combined frequency and time-shift keyed transmission systems. Commun Syst, IEEE Transact 1963;11(4):414–21.
[14] Falahati A, Woodward B, Bateman SC. Underwater acoustic channel models for 4800 b/s QPSK signals. IEEE J Ocean Eng 1991;16(1):12–20.
[15] Falahati A, Bateman SC, Woodward B. A simulation model of fading in an underwater channel. IWW Dig; 1988(No. 80). p. 6/1–4.
[16] Xu J. Underwater acoustic voice communication. Xiamen: Xiamen University; 2001.
[17] Marcum J. A statistical theory of target detection by pulsed radar. Inform Theory, IRE Transact 1960;6(2):59–267.
[18] Changxin F, editor. Lectures on communication principles, 2nd ed. Publishing House of Electronics Industry; 2008.
[19] Proakis JG. Digital communications, 4th ed. McGraw-Hill; 2001.
[20] Simon MK, Alouini MS. Digital communication over fading channels-A unified approach to performance analysis, 1st ed. Wiley; 2000.